

## VARIATION OF THE SUBHALO ABUNDANCE IN DARK MATTER HALOS

TOMOAKI ISHIYAMA<sup>1,2</sup>, TOSHIYUKI FUKUSHIGE<sup>3</sup>, AND JUNICHIRO MAKINO<sup>1</sup>

<sup>1</sup> National Astronomical Observatory, Mitaka, Tokyo 181-8588, Japan; [ishiyama@cfca.jp](mailto:ishiyama@cfca.jp), [makino@cfca.jp](mailto:makino@cfca.jp)

<sup>2</sup> Department of General System Studies, College of Arts and Sciences, University of Tokyo, Tokyo 153-8902, Japan

<sup>3</sup> K&F Computing Research Co., Chofu, Tokyo 182-0026, Japan; [fukushig@kfcf.jp](mailto:fukushig@kfcf.jp)

Received 2008 December 3; accepted 2009 February 26; published 2009 April 28

### ABSTRACT

We analyzed the statistics of subhalo abundance of galaxy-sized and giant-galaxy-sized halos formed in a high-resolution cosmological simulation of a 46.5 Mpc cube with the uniform mass resolution of  $10^6 M_\odot$ . We analyzed all halos with mass more than  $1.5 \times 10^{12} M_\odot$  formed in this simulation box. The total number of halos was 125. We found that the subhalo abundance, measured by the number of subhalos with maximum rotation velocity larger than 10% of that of the parent halo, shows large halo-to-halo variations. The results of recent ultra-high-resolution runs fall within the variation of our samples. We found that the concentration parameter and the radius at the moment of the maximum expansion show fairly tight correlation with the subhalo abundance. This correlation suggests that the variation of the subhalo abundance is at least partly due to the difference in the formation history. Halos formed earlier have a smaller number of subhalos at present.

**Key words:** cosmology: theory – galaxies: dwarf – methods: *N*-body simulations

### 1. INTRODUCTION

The cold dark matter (CDM) model is widely accepted as the standard theory of the formation and evolution of the universe. According to this CDM model, the structure formation in the universe proceeds hierarchically, from small-scale structures to larger-scale ones.

The CDM model successfully reproduced large-scale structures (e.g., Davis et al. 1985; Springel et al. 2005). However, it has been claimed that there are serious discrepancies between the structure predicted by the CDM model and that observed, in the scale of galaxy-sized objects and below.

Moore et al. (1999a) and Klypin et al. (1999) calculated the evolution of galaxy-scale dark matter halos using high-resolution cosmological *N*-body simulations. They found that dark matter halos of the mass comparable to the Local Group contained far too many subhalos compared to the number of known dwarf galaxies in the Local Group. In the case of dark matter halos of the size of typical clusters of galaxies, the theoretical prediction and observation agreed pretty well. The theoretical prediction for galaxy-sized and cluster-sized halos are similar, and observations of clusters of galaxies and that of Local Group are very different.

This discrepancy, now called “missing dwarf problem,” was studied by many researchers. Follow-up simulation studies (e.g., Diemand et al. 2004; Reed et al. 2005; Kase et al. 2007) gave essentially the same results as those of Moore et al. (1999a) and Klypin et al. (1999). Accordingly, it is now regarded as one of the most serious problems of the CDM model.

A number of solutions for this problem have been proposed. For example, we can reduce the number of subhalos in small scales by changing the nature of dark matter in small scales. Models in this direction are warm dark matter (Kamionkowski & Liddle 2000) and self-interacting dark matter (Spergel & Steinhardt 2000). Another direction is to explain the discrepancy as the difference between the number of nonobserved dark matter subhalos and that of observed satellite galaxies. Maybe not all subhalos host dwarf galaxies, or the measured velocity dispersion of dwarf galaxies might be much smaller than the rotation velocity of the parent subhalos. Models in this direction

includes the suppression of star formation by early reionization (Susa & Umemura 2004) and self-regulation of star formation in small halos (Stoehr et al. 2002; Kravtsov et al. 2004). However, none of these explanations are widely accepted as the clear-cut solution for the missing dwarf problem.

In almost all previous studies of substructures in dark-matter halos, the so-called re-simulation method has been used. In this method, one simulation is done in the following two steps. In the first step, a relatively large volume (for galaxy-sized halos typically a 50–100 Mpc cube) is simulated with low-mass resolution, and the candidate regions for high-resolution simulations are identified. In the second step, the selected regions are simulated with higher mass resolution. In practically all recent high-resolution simulations, this re-simulation method is used (Diemand et al. 2007, 2008; Stadel et al. 2008; Springel et al. 2008).

This re-simulation method allows us to resolve the structure of a selected halo with a very high resolution. On the other hand, it is not clear what kind of selection bias is introduced by the use of this method. Typically, the authors claimed that the halo, which looks similar to the halo of the Local Group, was selected to compare with the Local Group. However, in most cases the selection criteria were not described in detail, and thus it is difficult to see if any selection bias affected the results or not.

An obvious way to avoid the selection bias, which might be introduced by the use of the re-simulation method, is simply not to use it and do the high-resolution simulation of the entire initial simulation box. In Ishiyama et al. (2008, hereafter Paper I), we simulated a relatively small region (the size of the simulation box is 21.4 Mpc) with high-mass resolution (mass of particles =  $3 \times 10^6 M_\odot$ ). We identified 21 dark halos with maximum rotation velocity larger than  $200 \text{ km s}^{-1}$  and investigated the environmental effect on the subhalo abundance. The main conclusion of Paper I is that the abundance of subhalos has large variation. The most subhalo-rich halos contain the comparable number of subhalos as reported in Moore et al. (1999a), while least subhalo-rich ones contain around 1/10 subhalos. They also found that only the galaxy-sized halos (mass less than  $3 \times 10^{12} M_\odot$ ) show large variation in subhalo abundance, and

more massive ones show much smaller variation. The subhalo abundance shows correlation with the concentration parameter  $c$  (larger  $c$ , smaller abundance) and measures of the local density such as the smoothed local density and distance to the nearest massive halo.

The accuracy of the result of Paper I is, however, limited by both the mass resolution (particle mass  $3 \times 10^6 M_\odot$ ) and small number statistics. The total number of halos we analyzed was 21, and only 10 had the mass less than  $3 \times 10^{12} M_\odot$ . In this paper, we report the result of much larger, and thus much more accurate, simulation than that in Paper I. We simulated a box of the size 46.48 Mpc with  $1600^3$  particles of mass of  $1 \times 10^6 M_\odot$ . We also reduced the softening parameter from 1.8 kpc to 700 pc. Thus, compared to the calculation in Paper I, we used three times better mass resolution, two times better spatial resolution, and 10 times larger simulation volume. We identified all halos with the maximum rotation velocity larger than 160 km s<sup>-1</sup> and the virial mass  $M$  in the range of  $1.5 \times 10^{12} M_\odot \leq M < 1 \times 10^{13} M_\odot$ . We found 125 such halos. In all halos, the number of particles in the virial radius is more than  $1.5 \times 10^6$ , which is large enough to give reliable results for the statistics of subhalos with rotation velocity more than 1/10 of that of the parent halo (Kase et al. 2007).

In Section 2, we describe the initial model and the simulation method. In Section 3, we present the result. Section 4 presents summary and discussion.

## 2. INITIAL MODEL AND NUMERICAL METHOD

We adopted a  $\Lambda$ CDM ( $\Omega_0 = 0.3$ ,  $\lambda_0 = 0.7$ ,  $h = 0.7$ ,  $\sigma_8 = 0.8$ ) cosmological model for all of our calculations. In the largest simulation (simulation I), we used a cube of the comoving size of 46.48 Mpc and periodic boundary condition as the simulation box. The number of particles is  $1600^3$  and the mass of one particle is  $10^6 M_\odot$ . To generate initial particle distributions, we used the MPGRAFIC package (Prunet et al. 2008), which is a parallelized variation of the GRAFIC package (Bertschinger 2001). The initial redshift was 65.

For the time integration, we used the GreeM code (T. Ishiyama et al. 2009, in preparation), which is a massively parallel TreePM code based on the parallel TreePM code of Yoshikawa & Fukushige (2005). It uses the recursive multisection algorithm (Makino 2004) modified to achieve better load balancing for domain decomposition and the Phantom GRAPE special force calculation code (Nitadori et al. 2006) modified for the force with cutoff. The number of the grid points for PM calculation was  $400^3$ . The opening parameter of the tree part was  $\theta = 0.30$  up to  $z = 10$ , and was  $\theta = 0.50$  from  $z = 10$  to  $z = 0$ .

We integrated the system using a leapfrog integrator with shared and adaptive time steps. The step size was determined as  $\min(2.0\sqrt{\varepsilon}/|\vec{a}_i|, 2.0\varepsilon/|\vec{v}_i|)$  (minimum of these two values for all particles). The total number of time steps was 15,844. The (plummer) gravitational softening  $\varepsilon$  was constant in the comoving coordinate up to  $z = 10$ , and was constant (700 pc) in the physical coordinate from  $z = 10$  to  $z = 0$ .

We used 2048 CPU cores on the Cray-XT4 at Center for Computational Astrophysics, CfCA, of National Astronomical Observatory of Japan. The calculation time per step was about 60 s. The full run (15,844 time steps) was completed in 280 hr (wallclock time).

In order to investigate the effect of the spatial resolution, we performed two additional simulations (simulations S1 and S2). We used the same initial condition for these two runs and

**Table 1**  
Run Parameter

Parameter	Sim I	S1	S2
$N$	$1600^3$	$800^3$	$800^3$
$L$ (Mpc)	46.48	23.24	23.24
$\varepsilon$ (pc)	700	700	350
$N_{\text{step}}$	15844	10278	20513
$z_s$	10	10	21

changed the softening parameter. In Table 1, we summarize the number of particles  $N$ , the box size  $L$ (Mpc), the softening  $\varepsilon$ (pc), the number of steps  $N_{\text{step}}$ , and the redshift  $z_s$  after which the softening was constant in the physical coordinate, for the three simulations.

The method to find halos and subhalos is the same as that used in Paper I. Our method is based on the idea of finding all local potential minima. The identification of the main halos is done in the following three steps. In the first step, we sampled particles randomly according to the sampling rate  $R_{\text{samp}}$ , and calculated their potential. In this stage, all sampled particles are candidates for the centers of halos. Next, we select the particle with the smallest (most negative) potential and list it as the center of a halo. We then remove  $n_{\text{min}}$  neighbor particles of this center of halo particles from the original list of all particles, and select the potential minimum particle from the remaining particles. At this time, we again look at  $n_{\text{min}}$  neighbor particles from the list of originally selected particles, and if one of the neighbors has smaller potential, we do not add this particle to the list of halos. However, we remove  $n_{\text{min}}$  neighbors no matter if the particle is added to the list of halos or not. We repeat this procedure until there are no remaining particles. Next, we calculated the halo virial radius  $R_v$  in which the spherical overdensity is  $178\Omega_0^{0.4}$  times the critical value (Eke et al. 1996), the halo virial mass  $M$  and the maximum rotation velocity  $V_p$ . For identifying the main halos, we set  $R_{\text{samp}} = 0.01$  and  $n_{\text{min}} = 1000$  (this value corresponds to  $1.0 \times 10^{11} M_\odot$ ).

The method of finding the subhalos is almost the same as that for parent halos. The difference is that we do not reduce the particles. We detected all local potential minima inside the halo virial radius  $R_v$  as subhalos. For identifying the subhalos, we set  $n_{\text{min}} = 100$  (this value corresponds to  $1.0 \times 10^8 M_\odot$ ).

## 3. RESULT

We analyzed all halos with the maximum rotation velocity larger than 160 km s<sup>-1</sup> and the virial mass  $1.5 \times 10^{12} M_\odot \leq M < 1 \times 10^{13} M_\odot$ . The rotation velocity is defined as the maximum value of  $v_{\text{cir}}(r) = \sqrt{GM(r)/r}$ . We found 68 galaxy-sized halos ( $1.5 \times 10^{12} M_\odot \leq M < 3 \times 10^{12} M_\odot$ ), and 57 giant-galaxy-sized halos ( $3 \times 10^{12} M_\odot \leq M < 1 \times 10^{13} M_\odot$ ).

### 3.1. Effect of the Spatial Resolution

Let us first discuss the reliability of our result. Since the current calculation used relatively large softening, the difference between the results of S1 and S2 runs indicates the numerical error of the main calculation. We analyzed 21 galaxy-sized halos and 13 giant-galaxy-sized halos in simulations S1 and S2. In these two runs, we changed only the softening and other parameters are all kept the same. The reason why we test the effect of the softening here is that we use the softening significantly larger than that in Kase et al. (2007), though comparable to what is used in Springel et al. (2008) for comparable mass resolution (simulation Aq-A-5).

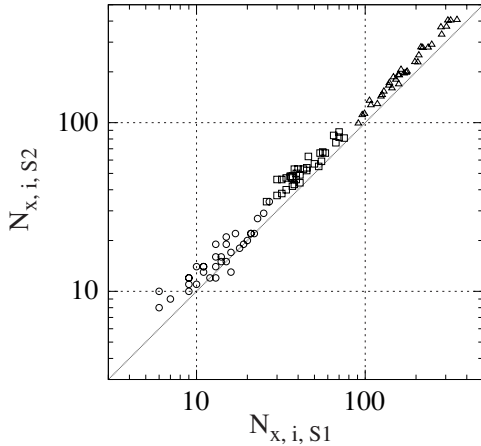


**Figure 1.** Number of subhalos of S1 plotted against those of S2. Here,  $N_{x,i,Sj}$  is the number of subhalos for halo  $i$  with normalized rotation velocity larger than  $x$ , in simulation  $Sj$ . Open circles, squares and triangles show  $N_{>0.15}$ ,  $N_{>0.10}$  and  $N_{>0.05}$ , respectively.

**Table 2**  
The Difference of the Subhalo Abundance

$x$	0.15	0.10	0.05
$\langle N_{x,i,S1} \rangle$	14.4	45.0	183.9
$\langle N_{x,i,S2} \rangle$	16.5	54.8	220.4
$\langle \Delta N_x / N_x \rangle$	0.175	0.233	0.190
$\langle (\Delta N_x / N_x)^2 \rangle^{1/2}$	0.246	0.258	0.200

It is known that subhalos contain less than 200 particles is not reliable (Kase et al. 2007). The subhalo abundances  $N_{>0.15}$ ,  $N_{>0.10}$  satisfy this condition. However,  $N_{>0.05}$  does not. Here,  $N_{>x}$  is defined as the number of subhalos with the maximum rotation velocity larger than  $x$  times that of their parent halos.

Figure 1 shows the subhalo abundance of individual halos in run S1 plotted against those for the same halos in run S2. Open circles, squares, and triangles show  $N_{>0.15}$ ,  $N_{>0.10}$ , and  $N_{>0.05}$ , respectively. We can see that halos in run S2 with smaller softening have more subhalos than their counterparts in run S1. The difference, however, is small.

Table 2 shows the average relative difference between the number of subhalos in run S1 and that in run S2, and their standard deviation. They are calculated as

$$\langle \Delta N_x / N_x \rangle = \frac{1}{n_{\text{halo}}} \sum_i \left( \frac{N_{x,i,S2}}{N_{x,i,S1}} - 1 \right), \quad (1)$$

$$\langle (\Delta N_x / N_x)^2 \rangle^{1/2} = \sqrt{\frac{1}{n_{\text{halo}}} \sum_i \left( \frac{N_{x,i,S2}}{N_{x,i,S1}} - 1 \right)^2}, \quad (2)$$

where  $n_{\text{halo}}$  is the number of halos and  $N_{x,i,Sj}$  is the number of subhalos for halo  $i$  with normalized rotation velocity larger than  $x$ , in simulation  $Sj$ . We can see that the deviation between the results of runs S1 and S2 is smallest for  $x = 0.05$ . This is partly due to small number statistics. As shown in Table 2, the number of subhalos is much smaller for higher rotation velocity.

The value of  $N_{0.05}$  is, however, not reliable because the number of particles in subhalos with this rotation velocity is too small. Therefore, we use the value  $N_{0.1}$  as the measure of the subhalo abundance. It does contain the error due to large softening, but as we have seen in this section that is small. So we ignore this error in the analysis given in this paper.

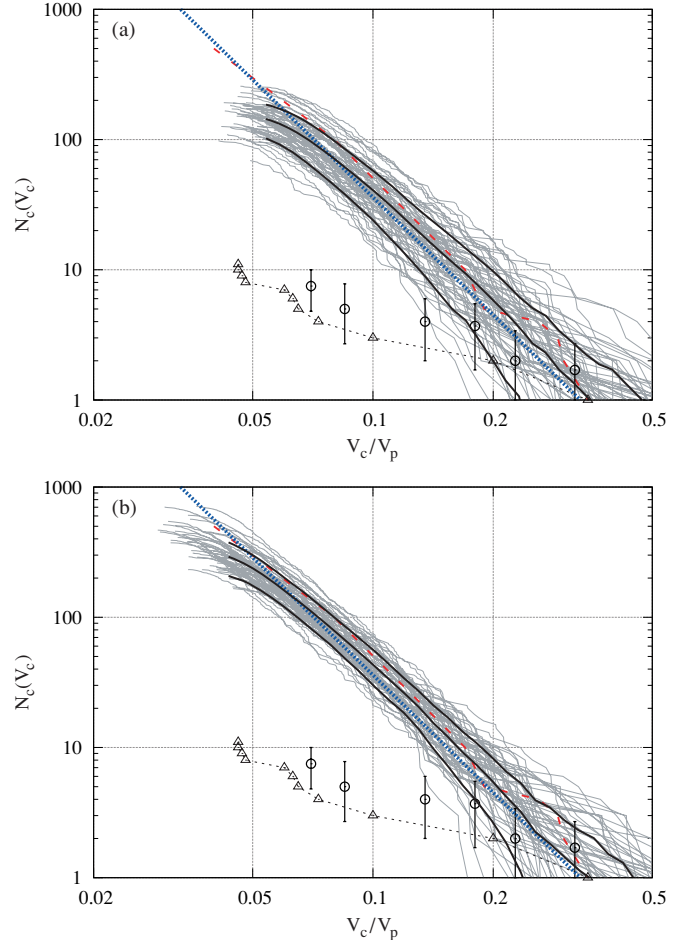


**Figure 2.** Cumulative numbers of subhalos as a function of their maximum rotation velocities  $V_c$  normalized by those of the parent halos  $V_p$ . (a) 68 galaxy-sized halos with  $1.5 \times 10^{12} M_\odot \leq M < 3 \times 10^{12} M_\odot$  (top). (b) 57 giant-galaxy-sized halos with  $3 \times 10^{12} M_\odot \leq M < 1 \times 10^{13} M_\odot$  (bottom). Three thick solid curves show the average (middle) and  $\pm 1\sigma$  values (top and bottom). Thick dotted and dashed curves are the fitting formula from Diemand et al. (2008) and the result of Moore et al. (1999a) for a galaxy-sized halo, respectively. The thin dashed curve with open triangles denotes the number of dwarf galaxies in our galaxy (Mateo 1998). The open circles with error bars show the number of dwarf galaxies in the Local Group (D'Onghia et al. 2007).

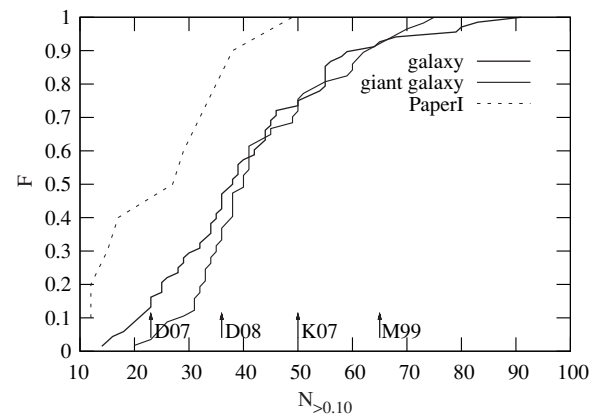


**Figure 3.** Cumulative function  $F$  of parent halos as a function of the number of subhalos with the normalized circular velocity larger than 0.1,  $N_{>0.1}$ . The thick solid curve shows the result for galaxy-sized halos. The thin solid curve shows the result for giant galaxy-sized halos. The thin dashed curve is for the result of Paper I. The arrows in the bottom show the results of several previous papers (D07: Diemand et al. 2007; D08: Diemand et al. 2008; K07: Kase et al. 2007; M99: Moore et al. 1999a).

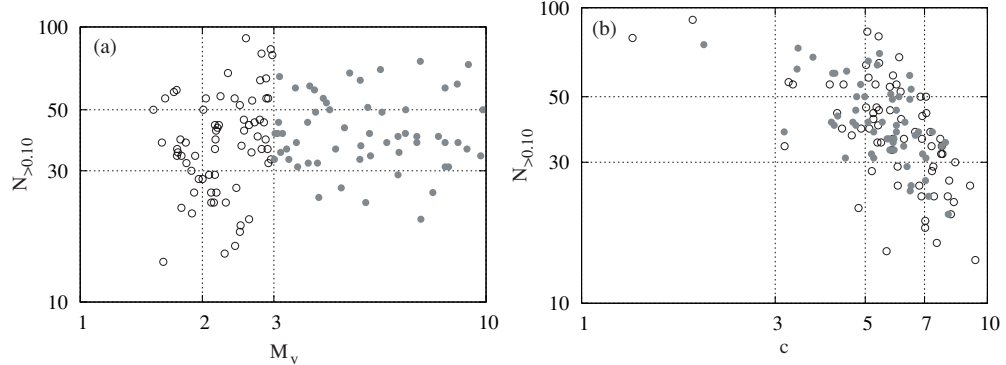


**Figure 4.** Dependence of the subhalo abundance  $N_{>0,10}$  on (a) mass  $M_{12}$  in unit of  $10^{12} M_\odot$  (left), (b) concentration parameter  $c = r_0/R_v$  (right). The white circles denote the halos with  $1.5 \times 10^{12} M_\odot \leq M < 3 \times 10^{12} M_\odot$ . The black circles denote the halos with  $3 \times 10^{12} M_\odot \leq M < 1 \times 10^{13} M_\odot$ .

### 3.2. Subhalo Abundance

Figure 2 shows the cumulative numbers of subhalos as a function of their maximum rotation velocities  $V_c$  normalized by those of the parent halos at  $z = 0$ . We can see that the variation of the subhalo abundance is significantly larger for galaxy-sized halos (the top panel) than for giant-galaxy-sized halos (the bottom panel). The result of Moore et al. (1999a) (thick dashed curve) is similar to those for our relatively subhalo-rich halos, while that of Diemand et al. (2008) (thick dotted curve) is comparable to our average value. The thin dashed curve with open triangles denotes the dwarf galaxies in our Galaxy (Mateo 1998), and open circles with error bars show the dwarf galaxies in the Local Group (D’Onghia et al. 2007). Note that these observational results do not include satellites recently found by SDSS (Willman et al. 2005; Belokurov et al. 2006; Zucker et al. 2006a, 2006b; Belokurov et al. 2007; Irwin et al. 2007; Walsh et al. 2007), and thus clearly are underestimates at least for the rotation velocity less than  $10 \text{ km s}^{-1}$  ( $V_c/V_p < 0.05$ ).

Figure 3 shows the cumulative distribution of the subhalo abundance of the parent halos. We used the number of subhalos with the normalized circular velocity larger than 0.1,  $N_{>0.1}$ , as the measure of the subhalo abundance. We can see that the variation of the subhalo abundance of galaxy-sized halo is larger than that for giant-galaxy-sized halos. The abundances of the richest halos are roughly the same for both galaxy-sized and giant-galaxy-sized halos, but the distribution of galaxy-sized halos is extended to smaller values of  $N_{>0.1}$ . We also show the result of several previous papers. The results of Kase et al. (2007) and Diemand et al. (2008) lie in the middle of the distribution of our halos, while the result of Moore et al. (1999a) corresponds to the richest ones. The differences of Moore et al. (1999a), Kase et al. (2007), and Diemand et al. (2008) are probably partly due to the difference in the cosmology. Moore et al. (1999a) and Kase et al. (2007) adopted standard CDM without  $\Lambda$ , while Diemand et al. (2008) used  $\Lambda$ CDM. Our present calculation and Diemand et al. (2008) used quite similar  $\Lambda$ CDM cosmological parameters. We will return to the question why the result of Diemand et al. (2007) corresponds to our most subhalo-poor halos in Section 4.1.

The dashed curve shows the result of Paper I, for galaxy-sized halos. The halos Paper I have somewhat smaller number of subhalos, but since there are only 10 galaxy-sized halos, the difference between Paper I result and the present result is well within the statistical variation (not significant for the KS test with 5% criterion).

### 3.3. The Cause of the Variation of Subhalo Abundance

Figure 4(a) shows the dependence of the parent halo on the mass. As already shown in Figure 2, the variation of the subhalo abundance of galaxy-sized halos is significantly larger than that for giant-galaxy-sized halos.

Figure 4(b) shows the dependence on the concentration parameter  $c$ . Here,  $c = r_0/R_v$ , where  $r_0$  is the scale radius of the fit to the Moore profile (Moore et al. 1999b), and  $R_v$  is the virial radius of the halo. The number of subhalos shows fairly tight correlation with the concentration parameter. More centrally concentrated halos have fewer subhalos. This correlation might mean that the subhalo abundance depends on the halo formation epoch. Halos with large values of  $c$  are generally formed earlier. This difference in the formation time might be the reason for the difference in the subhalo abundance.

In Paper I, we found dependences on the local density within 5 Mpc sphere normalized by the average density and also on the distance to the nearest influential larger-sized halo, which has three times or more mass of the parent halos. However, with the improved statistics of the present paper, we could not confirm these results.

Figures 5 and 6 show three subhalo-poor halos (top) and three subhalo-rich halos (bottom) at  $z = 6.04$ ,  $z = 3.21$ ,  $z = 1.04$ , and  $z = 0$  (left to right). They correspond to 0.85, 2.0, 5.68, and 13.7 Gyr. In Figure 6, only particles which lie in the halo virial radius at  $z = 0$  are plotted. As can be seen from the panels for  $z = 0$  in Figure 6, there is a large difference of the subhalo abundance. The large difference in the subhalo abundance is already clear at  $z = 1.04$ . At this moment, subhalo-poor halos have almost finished the assembling (except for the one in the top row, which still contains two large subhalos). On the other hand, subhalo-rich halos contain many more large halos which are in the process of first fallback. Moreover, they are part of much larger, Mpc-scale filamentary structures. In panels for  $z = 3.21$ , again, the difference between subhalo-poor halos and rich halos is rather clear. Rich ones contain many small structures scattered all over the distribution of particles which form the halo at  $z = 0$ . In the case of poor halos, at  $z = 3.21$  single high-density structure at the center is clearly visible.

When we compare the snapshot at high- $z$  in Figure 6, we can also see that the physical size of the distribution of particles is significantly smaller for poor halos, compared to rich halos. Also, the shape of the halo is smoother and rounder for poor halos.

Thus, from the way these halos are formed, as shown in Figures 5 and 6, it is rather clear why there is large variation in the

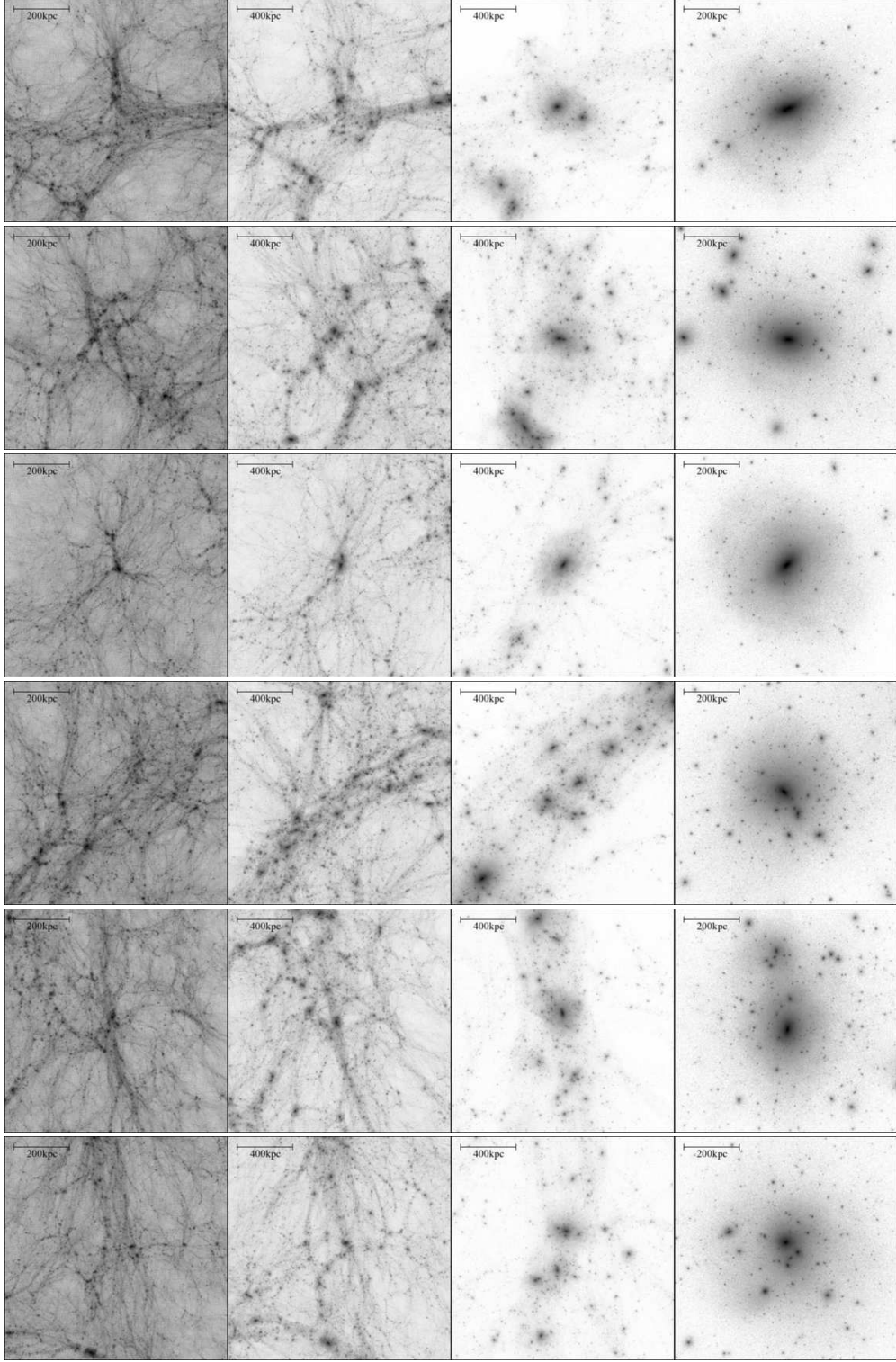


**Figure 5.** Snapshots of three subhalo-poor halos (top) and three subhalo-rich halos (bottom). Starting from the left, epoch are  $z = 6.04$ ,  $z = 3.21$ ,  $z = 1.04$ , and  $z = 0$ , width are 0.8 Mpc, 1.6 Mpc, 1.6 Mpc, and 0.8 Mpc. The center of snapshot is defined as the center of mass of particles which lie in the halo virial radius at  $z = 0.0$ .

subhalo abundance. Poor halos are formed from more centrally concentrated initial condition and formed earlier, while rich halos are formed from less concentrated structure and formed later.

In order to quantify the difference in the way the halos are formed, we tried many different measures, such as the time of the last major merger and the time at which the mass within the virial radius (or its certain fraction) exceeds 50% (or other

fraction) of the final mass. Most measures we tried show the correlation with the subhalo abundance, but that was weaker than that of the concentration parameter  $c$ . One measure with a fair success is the half-mass radius at the maximum expansion,  $R_{h,\max}$ , defined as the maximum value of the radius in which the half of the final virial mass is enclosed. To calculate this radius, we used the potential minimum as the center of the sphere.

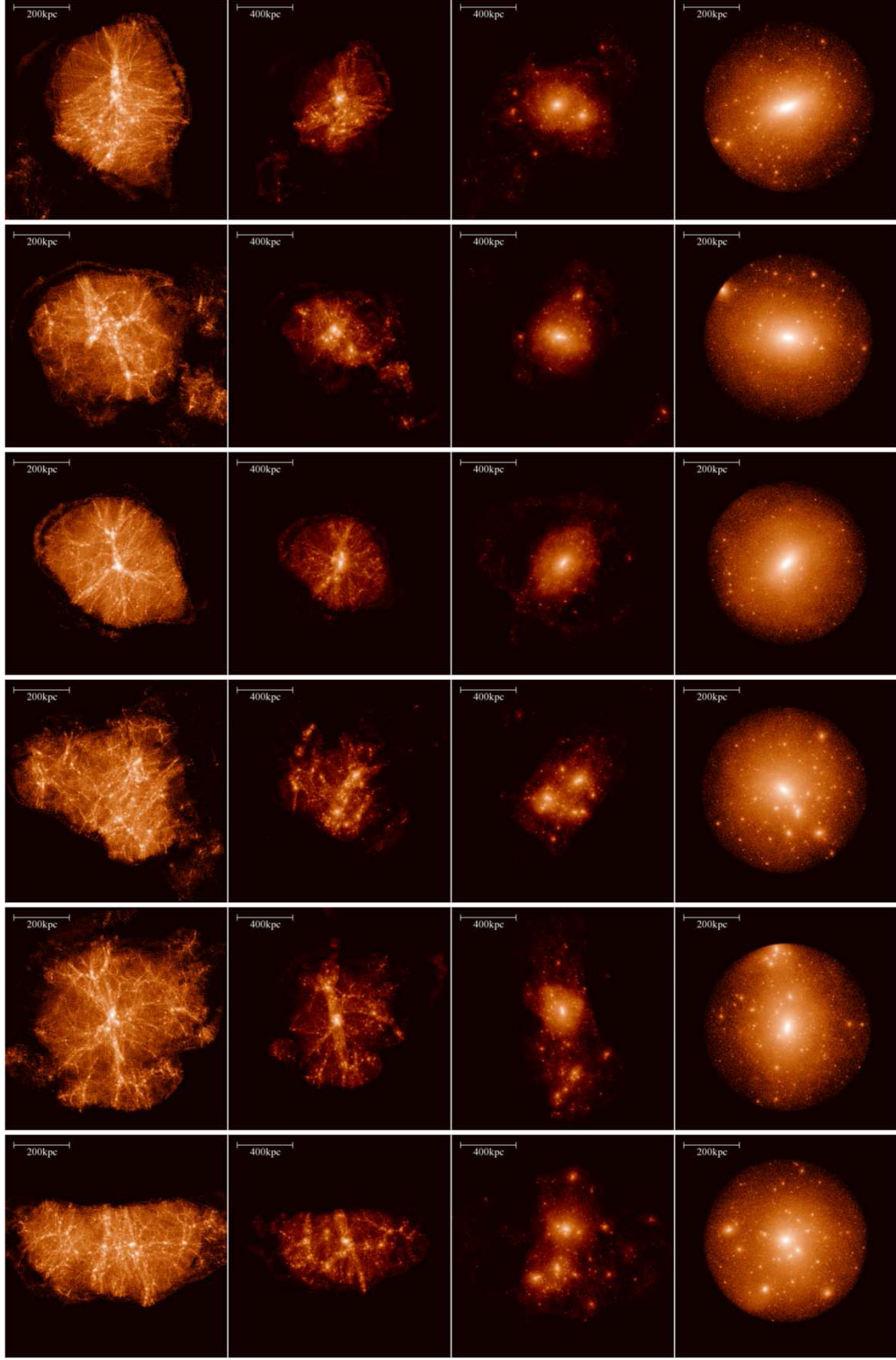


**Figure 6.** Same as Figure 5. However, only particles which lie in the halo virial radius at  $z = 0$  are plotted.

Figure 7 shows the evolution of the half-mass radius  $R_h$ . The solid and dashed curves show the results of the rich and poor halos, respectively.

We can see that  $R_h$  of poor halos reach the maximum values much earlier than those for rich halos, and the maximum values are smaller for poor halos. Also,  $R_h$  of poor halos seem to settle down faster than those of subhalo-rich halos.

Figure 8 shows the relation between the concentration parameter  $c$  and the maximum half-mass radius  $R_{h,\max}$  normalized by the halo virial radius  $R_v$  (left), and also  $N_{>0.1}$  and  $R_{h,\max}$ . We can see that the correlation is fairly tight for both cases. Thus, the number of subhalos is at least partly determined by the way the halo is assembled.

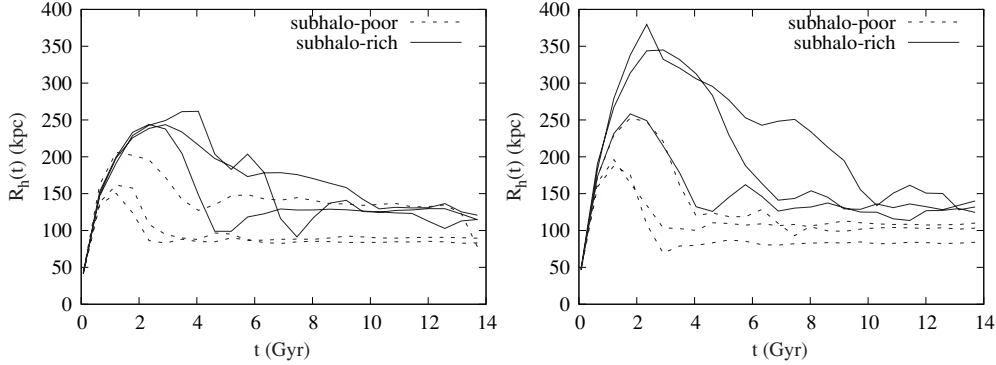


**Figure 7.** Evolution of the halo half-mass radius  $R_h(t)$ . The solid curves show the results of three subhalo-rich halos. The dashed curves show the results of three subhalo-poor halos. The left panel is for halos with  $1.5 \times 10^{12} M_\odot \leq M < 2.0 \times 10^{12} M_\odot$ . The right panel is for halos with  $2.0 \times 10^{12} M_\odot \leq M < 2.5 \times 10^{12} M_\odot$ .

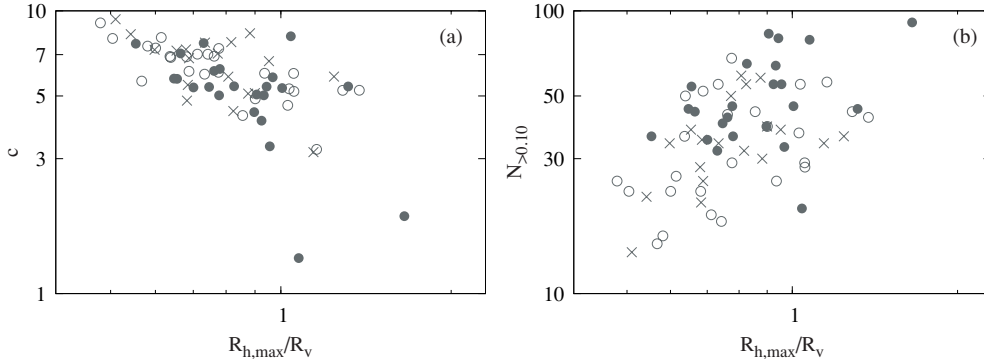


**Figure 8.** (a) Concentration  $c$  plotted against the maximum half-mass radius  $R_{h,\max}$  normalized by the halo virial radius  $R_v$  (left). (b) The subhalo abundance  $N_{>0.10}$  plotted against the maximum half-mass radius  $R_{h,\max}$  normalized by the halo virial radius  $R_v$  (right). Black circles, white circles, and crosses denote the halos with  $2.5 \times 10^{12} M_\odot \leq M < 3 \times 10^{12} M_\odot$ ,  $2.0 \times 10^{12} M_\odot \leq M < 2.5 \times 10^{12} M_\odot$ , and  $1.5 \times 10^{12} M_\odot \leq M < 2.0 \times 10^{12} M_\odot$ , respectively.

Figures 9–11 show three subhalo-poor halos (top) and three subhalo-rich halos (bottom) at  $z = 6.04$ ,  $z = 3.21$ ,  $z = 1.04$ , and  $z = 0$  (left to right). Their  $R_{h,\max}/R_v$  are almost same (upper to bottom, 0.71, 0.74, 0.68, 0.69, 0.78, 0.81) and their concentration parameter are also rather close (7.0, 7.0, 4.8, 6.1, 6.1, 5.9). Two of them are halos with  $1.5 \times 10^{12} M_\odot \leq M < 2.0 \times 10^{12} M_\odot$  (third and sixth from top). Others are halos with  $2.0 \times 10^{12} M_\odot \leq M < 2.5 \times 10^{12} M_\odot$ . However, we can see the large difference in the subhalo abundance from the panels for  $z = 0$  in Figure 11. As can be seen from the panels for  $z = 1.04$ , the difference of the shape of the halo is clear. At this moment, subhalo-poor halos have one or two large subhalos. By contrast, subhalo-rich halos have many small subhalos. In panels for high- $z$ , we can see the same feature for subhalo-poor and subhalo-rich halos as seen in Figure 6.

These mean that subhalo-poor halos with large maximum half-mass radius are formed from more centrally concentrated initial condition, formed earlier and have a small number of large companions. In such a halo, the maximum half-mass radius is large because of these companions. On the other hand, subhalo-rich halos have many small subhalos at  $z = 1.04$  and many merger events after that. This might be the reason for the large difference in the subhalo abundance of halos with same maximum half-mass radius.

#### 4. DISCUSSIONS AND SUMMARY

##### 4.1. Comparison with Aquarius Simulation

Springel et al. (2008) claimed that they found very small halo-to-halo variations in the subhalo abundance. They used the definition of the subhalo count different from what was used in

our work and most previous works. In this section, we compare our result with theirs.

Figure 12 shows the cumulative numbers of subhalos as a function of their maximum rotation velocities  $V_c$  normalized by the circular velocity of the parent halos at  $r_{50}$ . We define the radius  $r_{50}$  as that inside which the averaged spherical overdensity at 50 times the critical value and count the number of subhalos within  $r_{50}$ . This definition is the same as that used for Figure 10 in Springel et al. (2008). We plot the result of the 44 galaxy-sized halos with  $M_{50} < 3.0 \times 10^{12} M_\odot$ , where  $M_{50}$  is the mass within  $r_{50}$ .

If we measure the subhalo abundance again using  $N_{>0.1}$ , the number of subhalos with normalized rotation velocity more than 0.1, we can conclude that our result and Springel et al. (2008) result are practically identical. However, our results for  $N_{>0.1}$  may be affected by the resolution, because  $V_{50}$  is typically 20% smaller than the maximum rotation velocity  $V_p$ . Thus, our halos are probably slightly more subhalo-rich than those of Springel et al. (2008), but the halo-to-halo variation, calculated using the definition of Springel et al. (2008), is largely similar, though it is difficult to tell much on the variation in Springel et al. (2008) result because of small number of runs. We show three results here, and the total number of runs performed was six.

Compared with Figure 2, the variation of the subhalo abundance in Figure 12 is significantly smaller. This result is quite natural because of the two differences in the definition of the subhalo count. First, the use of  $r_{50}$  means that many subhalos are at the outermost region which are not virialized. Though subhalos in this outer region are gravitationally bound to the main halo, their evolution is not affected by the structure of the main halo simply because they are far from the central

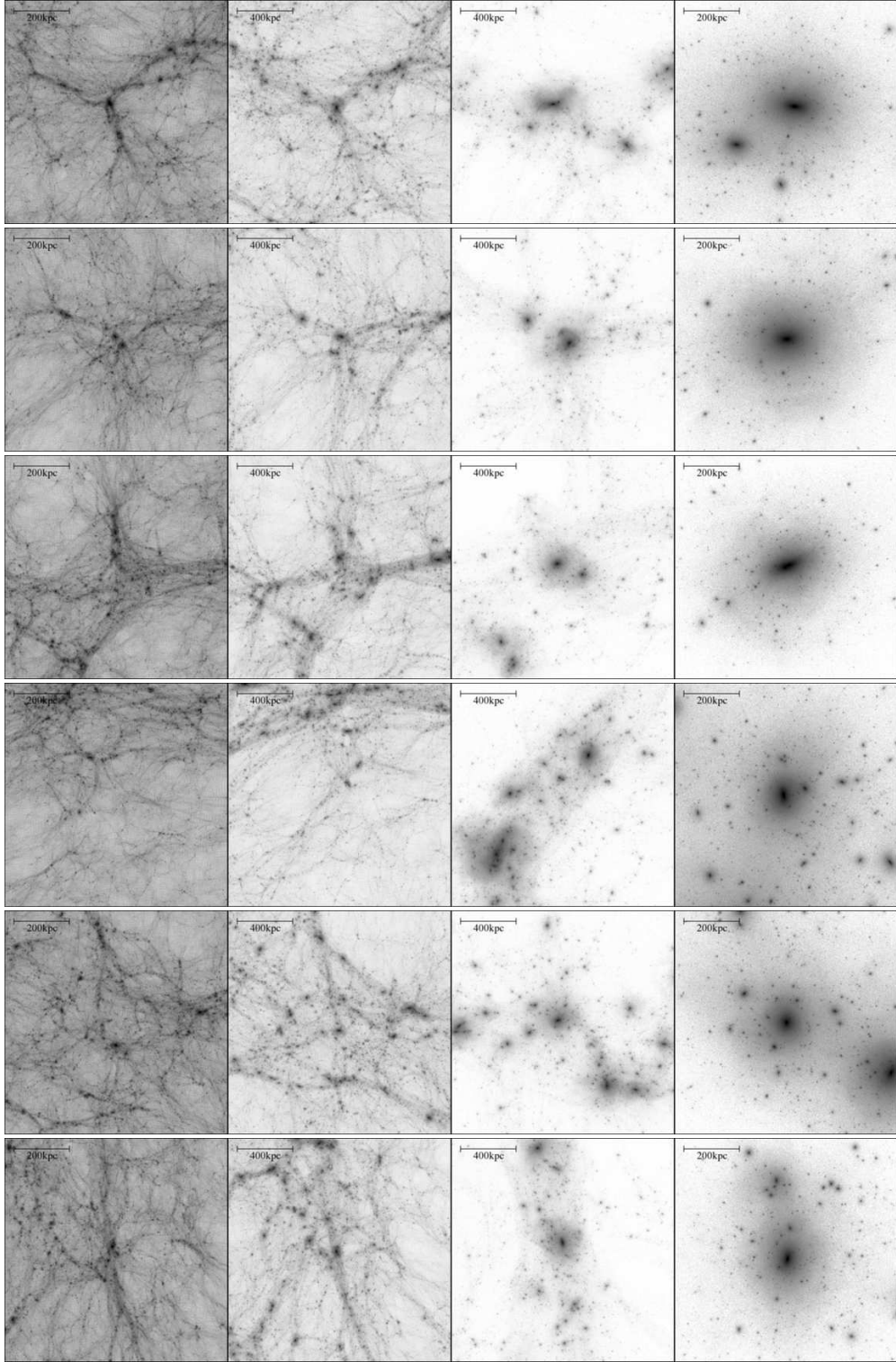


**Figure 9.** Snapshots of three subhalo-poor halos (top) and three subhalo-rich halos (bottom). Starting from the left, epoch are  $z = 6.04$ ,  $z = 3.21$ ,  $z = 1.04$ , and  $z = 0$ , width are 0.8 Mpc, 1.6 Mpc, 1.6 Mpc, and 0.8 Mpc. The center of snapshot is defined as the center of mass of particles which lie in the halo virial radius at  $z = 0.0$ .

high-density region. Second, the use of  $V_{50}$  instead of  $V_p$  would also reduce the halo-to-halo variation, since centrally concentrated halos have higher  $V_p$ .

Springel et al. (2008) claimed that the small halo-to-halo variation they found contradicted with the result of Paper I. Their rms halo-to-halo scatter was about 8%, while ours (in Figure 2) is about 41%. From the comparison above, it is clear that this

“contradiction” they found is partly due to the difference in the definition of the subhalo abundance. The halo-to-halo scatter as seen in Figure 12 is smaller than one in Figure 2. However, there is still some difference between our results and their ones. The remaining difference might be caused by their way to select parent halos. They selected the halos which host normal spirals in their semianalytic modeling.

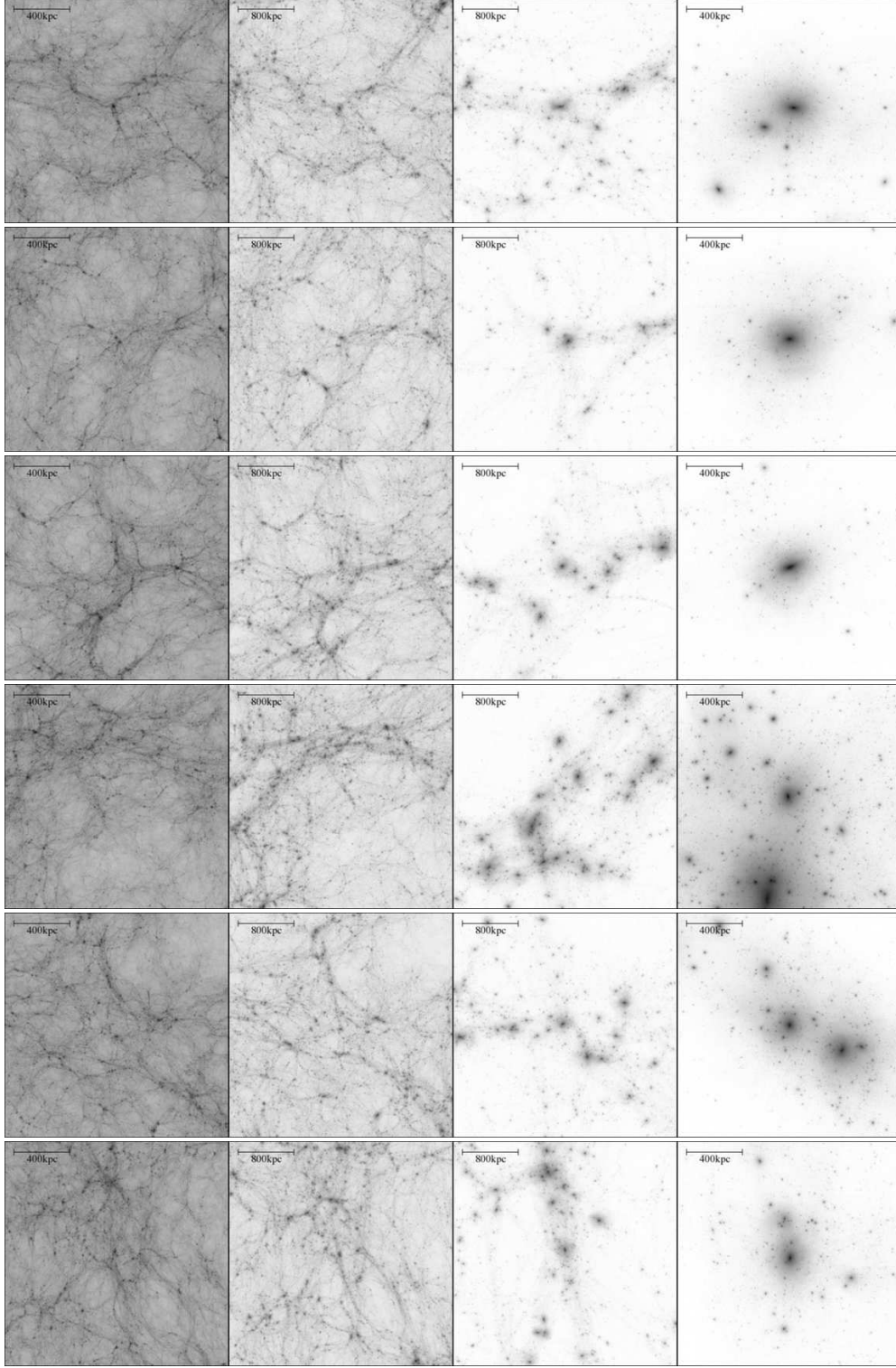


**Figure 10.** Same as Figure 9. However, Starting from the left, width are 1.6 Mpc, 3.2 Mpc, 3.2 Mpc, and 1.6 Mpc.

The systematic difference between Springel et al. (2008) results and our result may be due to the way Springel et al. (2008) selected their halos for high-resolution calculations. They selected halos without massive neighbors at  $z = 0$ , and they also put a criterion that in the semi-analytic calculation the halo should host a late-type galaxy. This would mean the selected halos should not experience major merger events at low- $z$ , and probably implies that their formation epoch is early. Thus, it is natural that their halos have systematically smaller

numbers of subhalos than ours have. They found systematic difference between their result and Via Lactea (Diemand et al. 2007, 2008) results. However, our result agrees with both.

#### 4.2. Is the Missing-dwarf Problem Solved?

The difference with the observed number of dwarf galaxies in Local Group or our galaxy is around a factor of 2 for the most subhalo-poor ones in our simulation, at the rotation

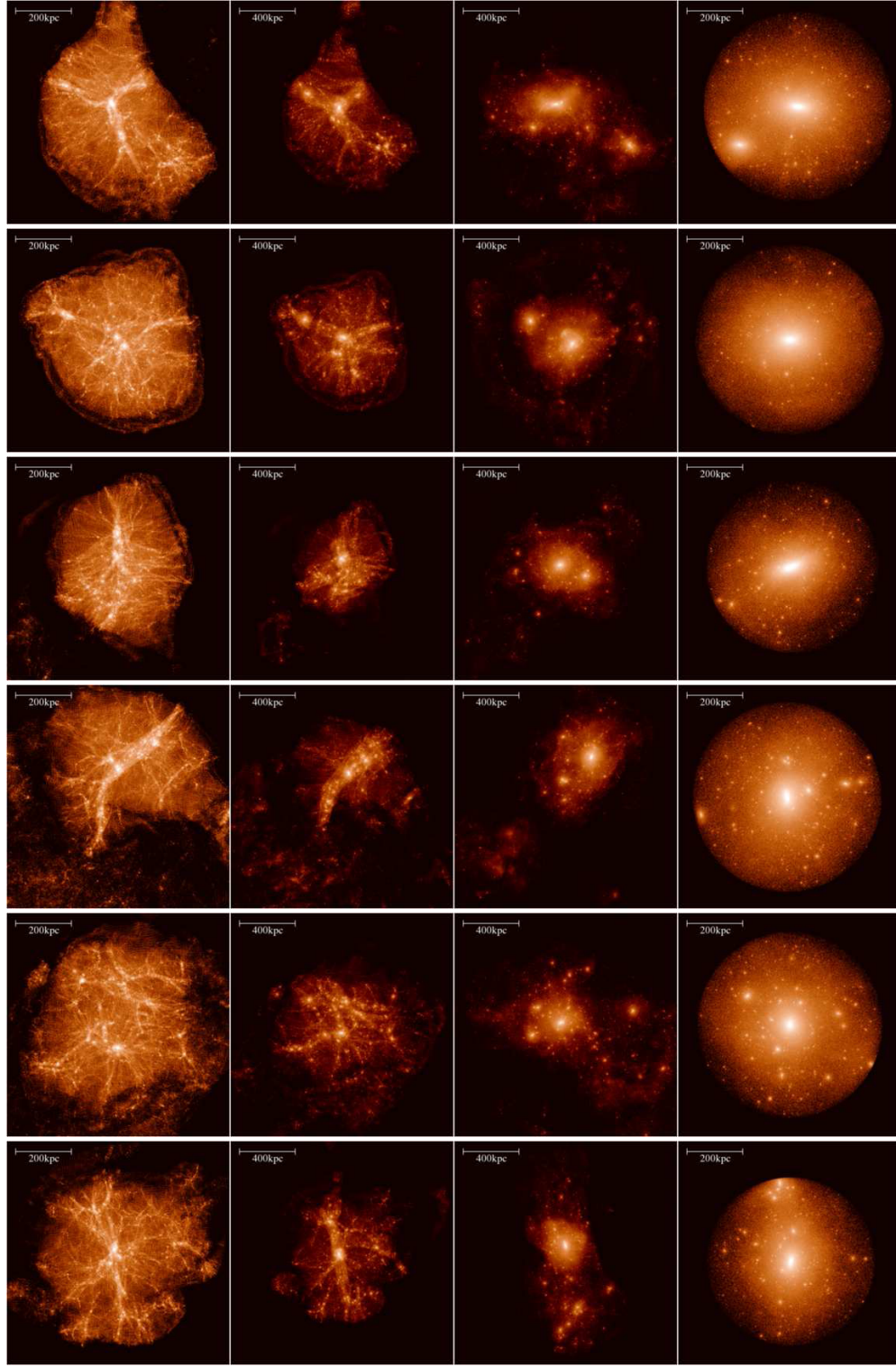


**Figure 11.** Same as Figure 9. However, only particles which lie in the halo virial radius at  $z = 0$  are plotted.

velocity 10% of that of the parent halo. For smaller velocities, the difference is larger, but recent SDSS results indicated that there are still many dwarf galaxies not identified. Thus, the missing dwarf problem does not seem to be a very serious problem. A factor-of-two difference may be easily explained by the effect of baryons. Also, Springel et al. (2008) found the subhalo abundance even lower than the lowest number we found. Thus, if our galaxy corresponds to most subhalo-poor halos

formed in  $\Lambda$ CDM universe, there is little discrepancy between the observed number of dwarf galaxies and the expected number of dark matter subhalos.

Obvious question is why our galaxy belongs to most subhalo-poor halos, but as we found the halos with high central concentration and early formation epoch have generally smaller number of subhalos. Also, since our galaxy is a spiral galaxy, it is unlikely that it experienced recent major merger event.

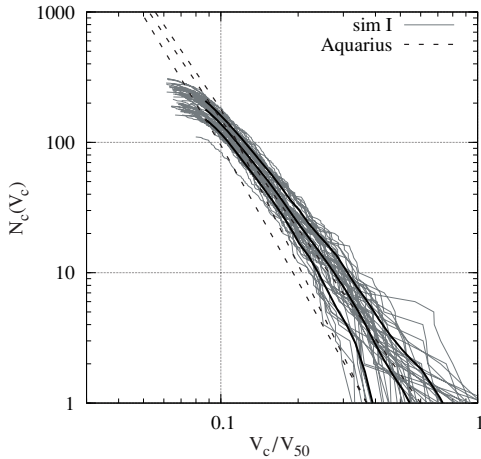


**Figure 12.** Cumulative numbers of subhalos as a function of their maximum rotation velocities  $V_c$  normalized by the circular velocity of the parent halos at  $r_{50}$ . Three thick solid curves show the average (middle) and  $\pm 1\sigma$  values (top and bottom). The thick dashed curves show the results of Springel et al. (2008, simulation Aq-A-1, Aq-C-2, Aq-E-2).

If we look at the Local Group as a whole, it will experience a major merger in some future, but in this case we should look at two main subhalos, our galaxy and M31, since their structure determine the total number of subhalos in the Local Group.

#### 4.3. Summary

We simulated  $1600^3$  particles with mass of  $1.0 \times 10^6 M_\odot$  in a  $46.48 \text{ Mpc}^3$  cubic box to create an unbiased sample of halos with resolution high enough to determine the abundance of subhalos. We confirmed the large variation of subhalo abundance we found in Paper I, but could not confirm the dependence on environmental parameters such as average density or distance to the nearest massive halo. However, we found clear dependence on the concentration parameter, which means the number of subhalos is determined primarily by the initial condition and formation time.

The “missing-dwarf problem” pointed out by Moore et al. (1999a) turned out to be much less serious, since now the discrepancy is around a factor of 2. A detailed study of baryon evolution of dwarf galaxies might be necessary to close up this remaining discrepancy.

We are grateful to Takayuki Saitoh for helpful discussions. We thank Keigo Nitadori for his technical advice. Numerical computations were carried out on Cray XT4 at Center for Computational Astrophysics, CfCA, of National Astronomical Observatory of Japan. This research is partially supported by the Special Coordination Fund for Promoting Science and Technology (GRAPE-DR project), Ministry of Education, Culture, Sports, Science and Technology, Japan.

#### REFERENCES

- Belokurov, V., et al. 2006, *ApJ*, **647**, L111
- Belokurov, V., et al. 2007, *ApJ*, **654**, 897
- Bertschinger, E. 2001, *ApJS*, **137**, 1
- Davis, M., Efstathiou, G., Frenk, C. S., & White, S. D. M. 1985, *ApJ*, **292**, 371
- Diemand, J., Kuhlen, M., & Madau, P. 2007, *ApJ*, **657**, 262
- Diemand, J., Kuhlen, M., Madau, P., Zemp, M., Moore, B., Potter, D., & Stadel, J. 2008, *Nature*, **454**, 735
- Diemand, J., Moore, B., & Stadel, J. 2004, *MNRAS*, **352**, 535
- D’Onghia, E., Maccio’, A. V., Lake, G., Stadel, J., & Moore, B. 2007, arXiv:0704.2604
- Eke, V. R., Cole, S., & Frenk, C. S. 1996, *MNRAS*, **282**, 263
- Irwin, M. J., et al. 2007, *ApJ*, **656**, L13
- Ishiyama, T., Fukushige, T., & Makino, J. 2008, *PASJ*, **60**, L13
- Kamionkowski, M., & Liddle, A. R. 2000, *Phys. Rev. Lett.*, **84**, 4525
- Kase, H., Makino, J., & Funato, Y. 2007, *PASJ*, **59**, 1071
- Klypin, A., Kravtsov, A. V., Valenzuela, O., & Prada, F. 1999, *ApJ*, **522**, 82
- Kravtsov, A. V., Gnedin, O. Y., & Klypin, A. A. 2004, *ApJ*, **609**, 482
- Makino, J. 2004, *PASJ*, **56**, 521
- Mateo, M. L. 1998, *ARA&A*, **36**, 435
- Moore, B., Ghigna, S., Governato, F., Lake, G., Quinn, T., Stadel, J., & Tozzi, P. 1999a, *ApJ*, **524**, L19
- Moore, B., Quinn, T., Governato, F., Stadel, J., & Lake, G. 1999b, *MNRAS*, **310**, 1147
- Nitadori, K., Makino, J., & Hut, P. 2006, *New Astron.*, **12**, 169
- Prunet, S., Pichon, C., Aubert, D., Pogosyan, D., Teyssier, R., & Gottloeber, S. 2008, *ApJS*, **178**, 179
- Reed, D., Governato, F., Quinn, T., Gardner, J., Stadel, J., & Lake, G. 2005, *MNRAS*, **359**, 1537
- Spergel, D. N., & Steinhardt, P. J. 2000, *Phys. Rev. Lett.*, **84**, 3760
- Springel, V., et al. 2005, *Nature*, **435**, 629
- Springel, V., et al. 2008, *MNRAS*, **391**, 1685
- Stadel, J., Potter, D., Moore, B., Diemand, J., Madau, P., Zemp, M., Kuhlen, M., & Quilis, V. 2008, arXiv:0808.2981
- Stoehr, F., White, S. D. M., Tormen, G., & Springel, V. 2002, *MNRAS*, **335**, L84
- Susa, H., & Umemura, M. 2004, *ApJ*, **610**, L5
- Walsh, S. M., Jerjen, H., & Willman, B. 2007, *ApJ*, **662**, L83
- Willman, B., et al. 2005, *ApJ*, **626**, L85
- Yoshikawa, K., & Fukushige, T. 2005, *PASJ*, **57**, 849
- Zucker, D. B., et al. 2006a, *ApJ*, **643**, L103
- Zucker, D. B., et al. 2006b, *ApJ*, **650**, L41